Transport of α-Helical Peptides through α-Hemolysin and Aerolysin Pores[†]

Radu Stefureac,[‡] Yi-tao Long,[‡] Heinz-Bernhard Kraatz,*[,§] Peter Howard,[||] and Jeremy S. Lee*[,‡]

Departments of Biochemistry, Chemistry, and Microbiology, University of Saskatchewan, Saskatoon, Saskatchewan S7N 5E5, Canada

Received March 10, 2006; Revised Manuscript Received May 9, 2006

ABSTRACT: A series of negatively charged α-helical peptides of the general formula fluorenylmethoxycarbonyl (Fmoc)-$D_xA_yK_z$ were synthesized, where *x* and *z* were 1, 2, or 3 and *y* was 10, 14, 18, or 22. The translocation of the peptides through single pores, which were self-assembled into lipid membranes, was analyzed by measuring the current blockade i_{block} and the duration t_{block}. The pores were either α-hemolysin, which has a wide vestibule leading into the pore, or aerolysin, which has no vestibule but has a longer pore of a similar diameter. Many thousands of events were measured for each peptide with each pore, and they could be assigned to two types: bumping events (type I) have a small i_{block} and long t_{block}, and translocation events (type II) have a larger i_{block} and shorter t_{block}. For type-II events, both i_{block} and t_{block} increase with the length of the peptides on both pores tested. The dipole moment and the net charge of each peptide has a major effect on the transport characteristics. The ratio of type-II/type-I events increases as the dipole moment increases, and uncharged peptides gave mostly type-I events. The structural differences between the two nanopores were reflected in the characteristic values of i_{block}, and in particular, the vestibule of α-hemolysin helps to orient the peptides for translocation. Overall, the results demonstrate that the nanopore technology can provide useful structural information but peptide sequencing will require further improvements in the design of the pores.

Bacterial pores, which have nanometer-scale openings, can be used as single-molecule detectors (*1*−*6*). The principle involves inserting the pore into a lipid membrane across which a voltage is applied and the ionic current is monitored. If a molecule enters the pore, the current is decreased by an amount and for a time, which is characteristic of the charge and structure of the molecule. The original work was performed with the α-hemolysin pore, which has a diameter of about 1.5 nm and will allow the transport of ssDNA but not dsDNA (*7*). Of considerable interest is the observation that polyA and polyU give different signals, leading to the possibility that the pore technology could be used for rapid nucleic acid sequencing (*8*−*10*). To achieve this goal, several groups have manufactured solid-state pores, which have the advantage of increased stability as well as the possibility of inserting other electronic detectors around the pore itself (*11*−*13*). Even so, many problems still remain, not the least of which is the high charge density of DNA and RNA, resulting in very fast transit times and loss of resolution. Recently, it was shown that the addition of glycerol could slow the DNA and lead to an order of magnitude improvement in the resolution (*14*).

The pore technology can also be used to analyze peptides and proteins. The interactions of cationic α-helical peptides with α-hemolysin have been explored (*15*). The effect of peptide charge and peptide length on the energy barrier for transport through the pore was measured. Previously, we have studied a series of collagen-like peptides, which existed as mixtures of single, double, or collagen-like triple helices. On the basis of the characteristic translocation parameters through α-hemolysin, we could distinguish and identify each peptide with the particular level of folding (*16*). Thus, structural information, which is difficult to obtain by bulk spectroscopic techniques, such as circular dichroism (CD)[1] or nuclear magnetic resonance (NMR), may also be available using the nanopores. As for sequencing, peptides in general have much lower charge densities, so that transit times are 1−2 orders of magnitude longer, giving rise to increased resolution compared to nucleic acids.

Here, we report the analysis of several α-helical peptides of the sequence fluorenylmethoxycarbonyl (Fmoc)-$D_nA_xK_y$ (see Table 1) through two nanopores. Peptides with this sequence have been previously synthesized, and the CD spectra have shown the formation of very stable α-helical secondary structures (*17*). Initially, we had intended to use the deprotected peptides, which have no net charge, but it soon became apparent that uncharged peptides give few translocation events. On the other hand, the Fmoc-protected peptides have a net negative charge, which allows them to be driven through the pore by the applied potential.

Two bacterial pores were used: α-hemolysin toxin from *Staphylococcus aureus* and aerolysin, a novel pore from the bacterium *Aeromonas hydrophila* (*18*−*21*). Schematic diagrams of the two pores are shown in Figure 1. The crystal

[†] Funding was provided by NSERC through discovery grants.

* To whom correspondence should be addressed. Telephone: 306-966-4660. E-mail: bernie.kraatz@usask.ca (H.-B.K.); Telephone: 306-966-4371. Fax: 306-966-4390. E-mail: leejs@usask.sask.ca (J.S.L.).

[‡] Department of Biochemistry.

[§] Department of Chemistry.

[||] Department of Microbiology.

[1] Abreviations: CD, circular dichroism; NMR, nuclear magnetic resonance; Fmoc, fluorenylmethoxycarbonyl.

10.1021/bi0604835 CCC: $33.50
Published on Web 07/04/2006

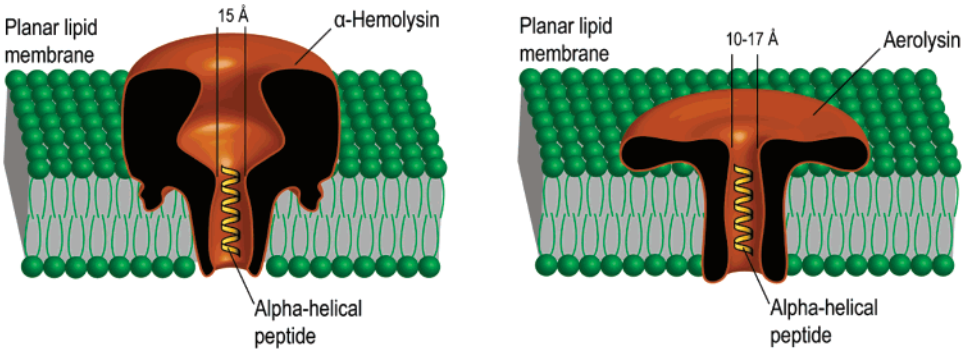

FIGURE 1: Schematic representation of the α-hemolysin and aerolysin pores inserted into planar lipid bilayers with linear α-helical peptides traversing the angstrom-sized channels.

Table 1: Sequence, Mass, Length, Dipole Moment, and Net Charge of the Examined Peptides

compound	mass	length (Å)[a]	dipole moment (Debye)[b]	net charge
Fmoc-$D_2A_{10}K_2$	1437	28.3	260	−1
Fmoc-$D_2A_{14}K_2$	1721	33.7	329	−1
Fmoc-$D_2A_{18}K_2$	2006	39.1	400	−1
Fmoc-$D_2A_{22}K_2$	2290	44.5	473	−1
Fmoc-$D_3A_{14}K_2$	1836	35.2	343	−2
Fmoc-$DA_{14}K$	1478	31.4	49	−1
$D_2A_{10}K_2$	1215	23.3	130	0

[a] The length of the peptide molecules was calculated from molecular-modeling simulations using Spartan software. [b] The dipole moments were calculated according to Creighton (*28*).

structure of α-hemolysin was solved in 1996, revealing a heptameric protein with a vestibule of 3 nm leading into the pore itself with a diameter of 1.5 nm (*22*). The charge transport characteristics are dominated by the narrowest constriction, but the vestibule may help to orient molecules before they enter the pore. No crystal structure is available for aerolysin, but a lower resolution electron microscopy study suggests that the two pores have similar diameters (*23*). However, aerolysin lacks the vestibule present in α-hemolysin and thus has a greater effective length. For ohmic behavior, the current through the nanopore is expected to be inversely proportional to the length, so that the open current for aerolysin will be smaller than for α-hemolysin under identical conditions (*24*). As shown below, this prediction is correct.

EXPERIMENTAL PROCEDURES

The peptides were synthesized by solid-phase synthesis on poly(ethylene glycol)−polystyrene resins using Fmoc chemistry (*25*). The product was cleaved off the resin and purified by using preparative reverse-phase high-performance liquid chromatography (HPLC) and characterized by time-of-flight mass spectrometry (Table 1). The measured mass was within ±1 mass unit of the calculated mass in all cases. To allow for further modification at the N terminus, the Fmoc group was initially left on. The deprotected peptides were prepared by treatment with piperidine and further purified by HPLC. CD measurements for Fmoc-$D_2A_{10}K_2$ and Fmoc-$D_2A_{22}K_2$ in 1 M KCl (see Figure S1 in the Supporting Information) confirmed the α-helical secondary structure previously reported by Perutz et al. for $D_2A_{10}K_2$ (*17*). Thus, the presence of the Fmoc group does not cause structural changes or extensive aggregation. Stock peptide solutions were prepared at 20 mg/mL.

α-Hemolysin was purchased from Sigma−Aldrich (St. Louis, MO) and used without purification. KCl, NaH_2PO_4, Na_2HPO_4, and decane were purchased from Aldrich (St. Louis, MO) and used as received. Diphytanoyl-phosphatidylcholine in $CHCl_3$ was purchased from Avanti Polar Lipids, Inc. (Alabaster, AL). Millipore water (18 MΩ cm) was used in all solutions. The $CHCl_3$ lipid solution was dried under a vacuum for 4 h and then redisolved in decane to a final concentration of 30 mg/mL of lipid. The electrolyte solution used throughout all bilayer measurements was 1.0 M KCl in 10 mM phosphate buffer (pH 8). The α-hemolysin solution was made up to a final concentration of 1.25 μg/mL and was stored at 4 °C. The aerolysin solution concentration was 1.5 μg/mL and contained 0.1 μM trypsin for activation and was stored at −20 °C. The bilayer cup and chamber were purchased from Warner Instruments (Hamden, CT). The perfusion cup has a volume of 1.5 mL and an aperture of 150 μm. Before bilayer formation, the decane−lipid suspension was applied on the aperture with a small paintbrush. The lipid excess was dried under a jet of argon. The two compartments of the bilayer cell, termed cis and trans, were encased in a block of solid copper that rested on an active-air-floating table (Kinetic Systems, Boston, MA) placed inside a Faraday cage (Warner Instruments). Both compartments were filled with 1.5 mL of electrolyte. Bilayers were formed by dipping the paintbrush into the lipid solution and painting across the aperture. Bilayer formation was monitored using capacitance measurements performed by PClamp 9.0. The multilayer was thinned to a bilayer with repeated brush strokes, until capacitance values allowing for pore insertion were obtained. A total of 5 μL of the respective pore solution was injected adjacent to the aperture in the cis chamber, and pore insertions were detected by a characteristic jump in current values. Once a stable single-pore insertion was detected, 10 μL of the 20 mg/mL stock peptide solutions was added to the 1.5 mL cis chamber, proximal to the aperture, giving a final peptide concentration of 0.13 mg/mL. The experiments were carried out at 22 ± 1 °C.

The bilayer experiments were run under voltage-clamp conditions using an Axopatch 200B amplifier (Axon Instruments, Union City, CA) connected to a CV 203BU headstage. A transmembrane negative potential of 100 mV was applied through Ag/AgCl electrodes. The signals were lowpass-filtered at 10 kHz with an eight-pole Bessel filter, digitized at 100 kHz by DigiData 1322A (Axon Instruments)

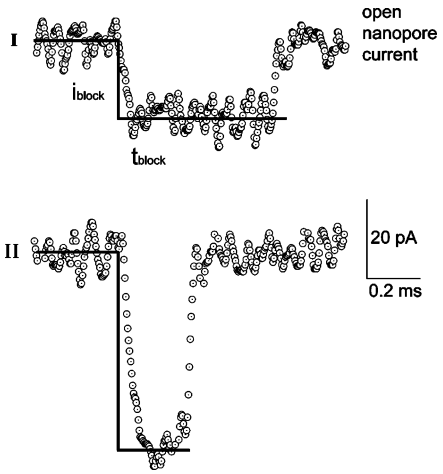

FIGURE 2: Two types of current blockade events on the aerolysin pore are shown by the open circles. Idealized blockade behavior is represented by the black line. i_{block} is the difference between the open nanopore current and the average amplitude of the blockade current. Also, the blockade duration, t_{block}, was determined from the idealized current trace.

and recorded by a PC running PClamp 9.0 (Axon Instruments). The applied negative potential of 100 mV drove anions from the cis to the trans chamber. Analysis of all data was performed by ClampFit 9.0 (Axon Instruments) and Origin 7.0 (OriginLab Corporation, Northampton, MA). The blockade current populations were obtained by fitting the blockade current distribution with the Gaussian function. The lifetime data were obtained by fitting each blockade duration distribution with a single-exponential function (26). Typical results for Fmoc-$D_2A_{10}K_2$ are shown in Figure S2 in the Supporting Information. The bin increments were set at 1 pA and 0.05 ms for the blockade current and duration, respectively.

RESULTS

Blockade Events. Upon formation of a stable lipid bilayer, there is a complete current blockade. Successful insertion of a single α-hemolysin or aerolysin pore resulted in open-pore currents of 100 or 50 pA, respectively. Initially, the deprotected peptides were studied; however, the rate of data acquisition was slow, and most of the events had small blockade currents (see Figure S3 in the Supporting Information). These peptides have no net charge, so that the interaction with the pore is diffusion-controlled. The Fmoc peptides, on the other hand, have a net negative charge and thus will be driven through the pores. Indeed, upon addition of Fmoc peptides to the cis side of the chamber, blockade events were witnessed immediately and, in general, many thousands of events could be recorded within 1 or 2 h before the bilayer broke down. For aerolysin, the blockade events were almost exclusively of two types as shown in Figure 2. Each event can be characterized by two parameters, the current blockade, i_{block}, and the blockade time, t_{block}, which were dependent upon the sequence of the peptide. In general, type-I events have a small i_{block} and a long t_{block}, whereas type-II events have a larger i_{block} and a smaller t_{block}. As discussed previously, type-I events with a small i_{block} are assigned to peptides that bump into the pore and then slowly diffuse away (*8*, *16*). Type-II events with a larger i_{block} are assigned to peptides that are transported through the pore. As described below, the ratio of type-I/type-II events was also dependent upon the sequence of the peptide. About 1−2% of events could not be assigned to either type I or II, but the majority of these appeared to be a small blockade followed by a larger blockade. The simplest interpretation would be a peptide that bumps into the pore and is then transported before it can diffuse away. However, such complex events were excluded from the analysis. For α-hemolysin, the open-pore current is larger, resulting in a better signal-to-noise ratio, and, except for peptide Fmoc-$DA_{14}K$, type-II events predominated.

Table 2: Peptide Translocation Parameters through Aerolysin[a]

compound	I_1 (pA)	I_2 (pA)	T_1 (ms)	T_2 (ms)	A_1	A_2	A_1/A_2	W_1	W_2
Fmoc-$D_2A_{10}K_2$	−17.0	−31.5	0.92	0.14	5863	4787	1.224	4.0	6.0
Fmoc-$D_2A_{14}K_2$	−17.5	−32.5	0.94	0.23	5342	7139	0.748	4.2	4.9
Fmoc-$D_2A_{18}K_2$	−18.1	−33.0	0.91	0.39	3029	6778	0.447	4.3	4.5
Fmoc-$D_2A_{22}K_2$	−26.3	−38.1	0.61	0.48	1710	10 738	0.159	3.5	3.0
Fmoc-$D_3A_{14}K_2$	−23.8	−42.6	0.68	0.25	2389	5957	0.401	4.3	6.1
Fmoc-$DA_{14}K$	−17.6	−35.0	0.88	0.16	2329	728	3.20	6.4	10.1

[a] I_1 and I_2 and T_1 and T_2 represent the intensities and durations of the current blockade for the events belonging to the first and second populations presented in Figure 3. A_1 and A_2 are the number of events of each population. W_1 and W_2 are the peak widths at half-height. The results are the averages of at least three independent measurements, and the standard deviations were less than 1% for I and less than 5% for T.

Aerolysin. Because the vast majority of events fall into two distinct types, we have chosen a simple analysis in which the number of events is counted for each 1 pA increment in i_{block}. The results for all six peptides are shown in Figure 3, and the averaged parameters from at least three independent experiments are listed in Table 2. In all cases, there is a single Gaussian distribution for both translocation and bumping events. Therefore, it would appear that only monomers are present in the peptide samples because dimers or other complexes would give rise to multiple types of events as was seen previously with collagen peptides (*16*). Alternatively, if complexes are forming, then they must be very weak and do not effect the translocation events. As discussed previously, the distribution of translocation times is not Gaussian and the value of t_{block} is best derived from an exponential fit (*26*). For Fmoc-$D_2A_{10}K_2$, the average i_{block} values for type-I (I_1) and type-II (I_2) events were −17.0 and −31.5 pA, respectively, with corresponding t_{block} values (T_1 and T_2) of 0.92 and 0.14 ms. In other words, a translocation event gives a blockade current that is about twice as large and a blockade duration that is about 6 times shorter compared to a bumping event. There are also more type-I (A_1) than type-II events (A_2) in the ratio of about 1.2:1.

The peptide Fmoc-$D_2A_{14}K_2$ contains an extra turn of the α helix, and the histogram of blockade currents appears very similar to that for Fmoc-$D_2A_{10}K_2$. However, there are a number of differences (Figure 3 and Table 2). First, there are small but significant increases in both I_1 and I_2. Because this peptide is larger, an increase in I_1 might be expected but the diameter is unchanged and, therefore, an increase in I_2 for transportation is not intuitively obvious (see the Discussion). Second, the change in T_1 is small, whereas T_2 increases significantly because a longer peptide takes longer to translocate. Third, the ratio of A_1/A_2 decreases to 0.75.

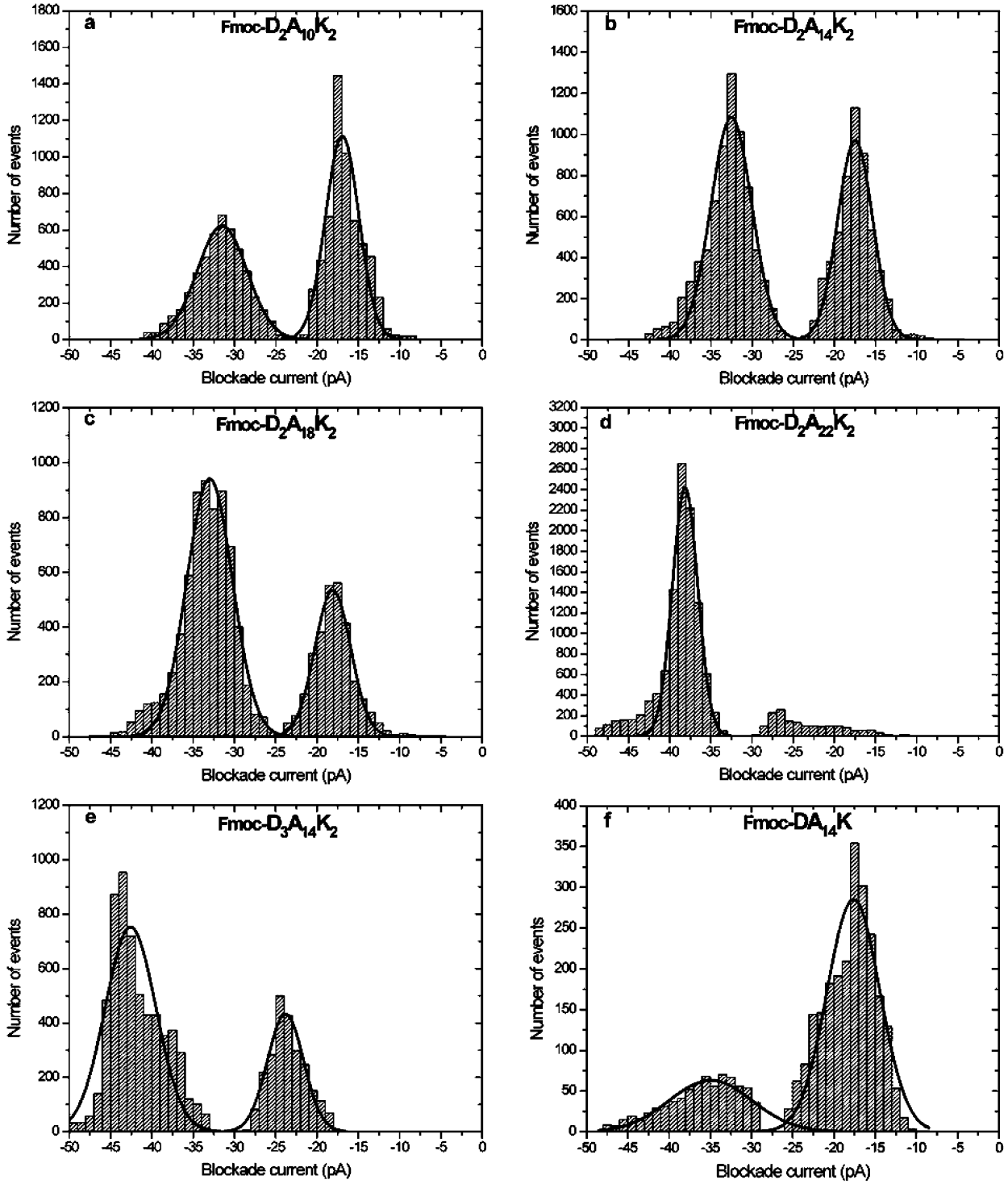

FIGURE 3: Histograms of the i_{peak} values collected for the six peptides tested on aerolysin pores.

Thus, for a longer peptide, more events result in translocation. As discussed below, a simple explanation is that the longer peptide has an increased dipole moment (Table 1). Fourth, W_2, the peak width at half-height for type-II events, is decreased. In other words, there is less variation in i_{block}, an effect that again can be ascribed to an increase in the dipole moment. For the longer peptides, Fmoc-$D_2A_{18}K_2$ and Fmoc-$D_2A_{22}K_2$, the same four trends are apparent. Specifically, there are increases in I_1, I_2, and T_2, a decrease in the ratio of A_1/A_2, and a decrease in the peak width, W_2.

The peptide, Fmoc-$D_3A_{14}K_2$, has one additional negative charge, and thus, translocation is favored by the voltage gradient across the pore. One effect of this was immediately apparent; there was a large increase in the number of events per unit time compared to Fmoc-$D_2A_{14}K_2$ presumably because of increased transport to the vicinity of the pore. Surprisingly, the translocation time T_2 is similar to that of the −1 peptide, and both I_1 and I_2 are increased. The value for I_2 was −42.6 pA, which is larger than that for the longest peptide Fmoc-$D_2A_{22}K_2$ (−38.1 pA). A decrease in the ratio of A_1/A_2 is again consistent with an increase in the dipole moment.

A more direct test of the effect of the dipole moment is provided by Fmoc-$DA_{14}K$, which has only one net negative

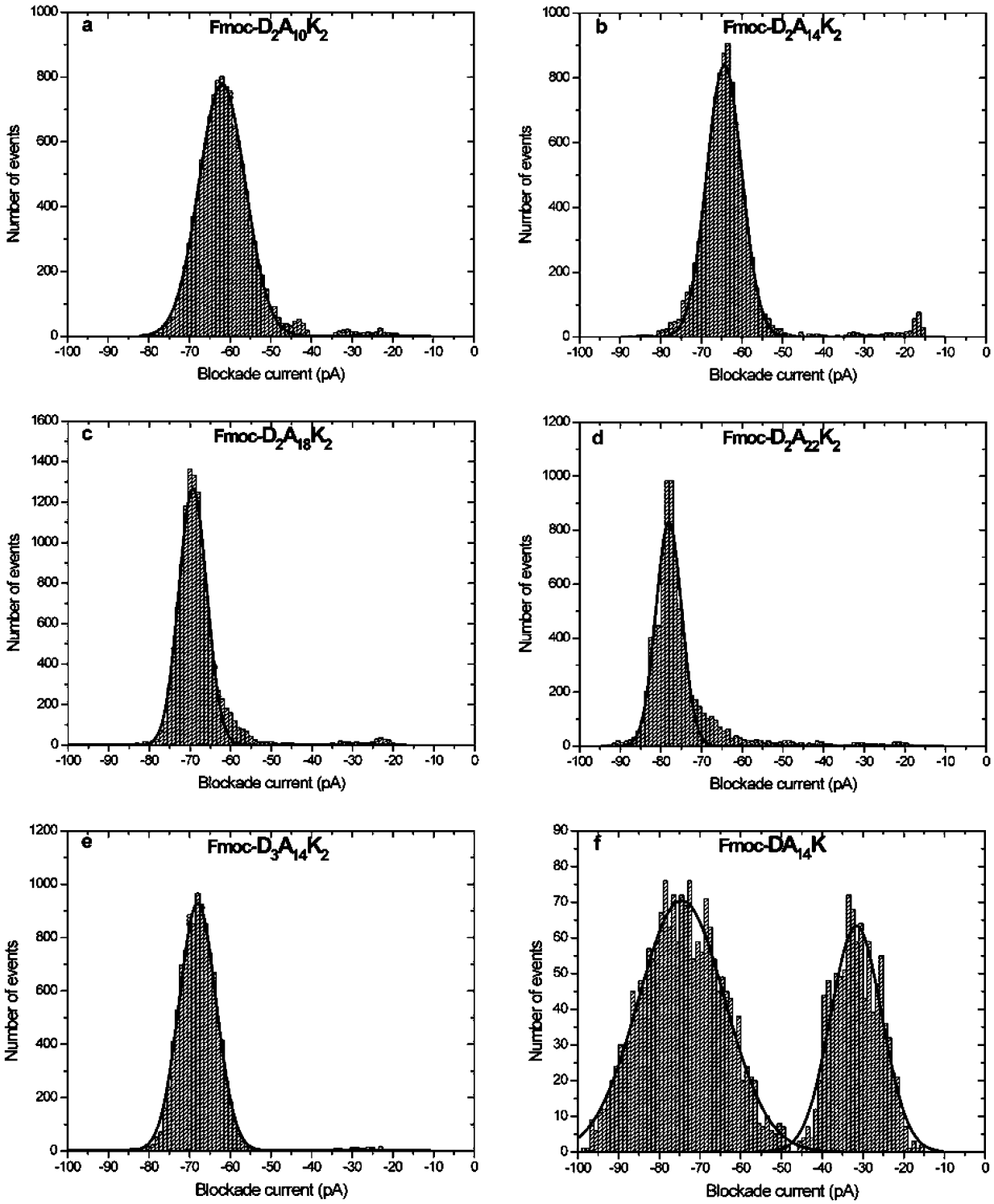

FIGURE 4: Histograms of the i_{peak} values collected for the six peptides tested on α-hemolysin pores.

charge but a very small dipole because of the inherent dipole of α helices (Table 1). As expected, there is a large increase in both the A_1/A_2 ratio and the peak width W_2, but the value of T_2 decreases significantly. We were unable to test a peptide such as A_{14}, which has no formal charge because of solubility problems.

α-*Hemolysin*. A similar analysis was performed with all six peptides using the α-hemolysin pore (Figure 4 and Table 3). As mentioned above, the open-pore current for α-hemolysin is 100 pA. One striking difference compared to the aerolysin pore is that there are very few type-I events with small i_{block} (because the numbers were so small, no statistical analysis was possible), except in the case of Fmoc-$DA_{14}K$. Di- and multimers of the peptide would be too large to fit through the pore. Thus, the lack of type-I events and a single Gaussian distribution again suggests that monomer peptides are being interrogated. In contrast to aerolysin, the α-hemolysin pore has a vestibule with a much larger diameter (Figure 1), which may help to guide any peptides in the vicinity into the narrow constriction of the pore itself.

Table 3: Peptide Translocation Parameters through α-Hemolysin[a]

compound	I_2 (pA)	T_2 (ms)	A_2	W_2
Fmoc-$D_2A_{10}K_2$	−62.0	0.19	11 329	11.1
Fmoc-$D_2A_{14}K_2$	−65.1	0.34	9501	8.3
Fmoc-$D_2A_{18}K_2$	−69.3	0.54	11 721	6.5
Fmoc-$D_2A_{22}K_2$	−78.1	0.65	7835	5.9
Fmoc-$D_3A_{14}K_2$	−68.0	0.21	10 502	8.8
Fmoc-$DA_{14}K$	$I_1 = -31.6$	$T_1 = 0.27$	$A_1 = 963$	$W_1 = 12.4$
	$I_2 = -74.5$	$T_2 = 0.25$	$A_2 = 1851$	$W_2 = 21.2$

[a] I_1 and I_2 and T_1 and T_2 represent the intensities and durations of the current blockade for the events belonging to the first and second populations presented in Figure 4. A_1 and A_2 are the number of events of each population. W_1 and W_2 are the peak widths at half-height. Of the six peptide molecules tested, only Fmoc-$DA_{14}K$ showed two well-defined event population distributions. The results are the averages of at least three independent measurements, and the standard deviations were less than 1% for I and less than 5% for T.

For the four peptides of increasing length, from Fmoc-$D_2A_{10}K_2$ to Fmoc-$D_2A_{22}K_2$, the I_2 increases from −62.0 to 78.1 pA and the T_2 increases from 0.19 to 0.65 ms. As was observed for aerolysin, the peak width also decreases significantly as the length increases. The −2 charged peptide, Fmoc-$D_3A_{14}K_2$, has an increased I_2 compared to Fmoc-$D_2A_{14}K_2$, but in contrast to the result with aerolysin, the T_2 decreases from 0.34 to 0.21 ms. Thus, changes to the charge of the peptide have effects that are dependent upon the structure of the pore. Finally, Fmoc-$DA_{14}K$, which has a small dipole, gives a significant number of type-1 events with a ratio of A_1/A_2 of about 0.5. The value of W_2 is also very large. As was the case with aerolysin for Fmoc-$DA_{14}K$, the translocation time T_2 is decreased and the blockade I_2 is increased compared to Fmoc-$D_2A_{14}K_2$.

Translocation Velocity. The t_{block} can be considered as the time it takes the peptide to pass the exit of the pore because, until it reaches the exit, the ions are still moving out of the pore. Thus, the velocity is simply the length of the polymer/t_{block}. It has been shown previously that for polymers that are shorter than the length of the pore the velocity decreases as the length increases. For longer polymers, the velocity is constant with length (*24*). For the four peptides of increasing length, from Fmoc-$D_2A_{10}K_2$ to Fmoc-$D_2A_{22}K_2$, the velocities are plotted in Figure 5. For all lengths, the velocities through aerolysin are faster than through α-hemolysin, suggesting that ionic and/or hydrophobic interactions between the peptide and pore are greater for α-hemolysin. For α-hemolysin and aerolysin, the limiting velocity would appear to be about 7 and 9 nm/ms, respectively.

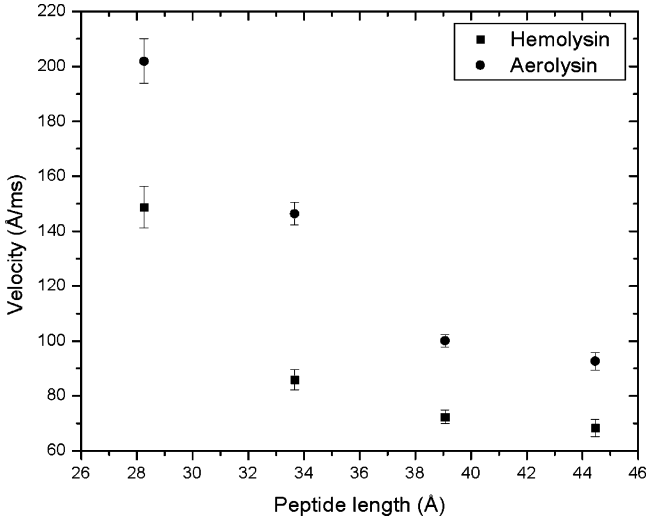

FIGURE 5: Translocation velocities of Fmoc-$D_2A_{10}K_2$, Fmoc-$D_2A_{14}K_2$, Fmoc-$D_2A_{18}K_2$, and Fmoc-$D_2A_{22}K_2$ peptides through α-hemolysin and aerolysin pores plotted as a function of their lengths. The velocities through aerolysin are faster than through α-hemolysin for all lengths, suggesting stronger interactions between the peptides and the α-hemolysin pore. The error bars show the standard deviation.

DISCUSSION

Comparison of the Two Pores. For α-hemolysin, the open current is 100 pA, whereas it is only 50 pA for aerolysin. However, this does not imply that the aerolysin pore is much smaller than α-hemolysin. The crystal structure of α-hemolysin is known (*22*), and the pore diameter is about 1.5 nm; however, only low-resolution structures are available for aerolysin (*23*). If it is assumed that both pores show ohmic conductance, then the open-pore current, I_{open}, can be written as $I_{open} = K(d^2)/L$, where K is a constant dependent upon the voltage and electrolyte resistance, d is the diameter of the pore, and L is the length of the pore (*27*). The α-hemolysin pore is about 5 nm in length, but the aerolysin pore lacks the vestibule and thus is about 8 nm in length (*23*). Therefore, we can calculate that $d_{hemolysin}/d_{aerolysin}$ is about 1.1, so that aerolysin has a diameter of about 1.4 nm, a value that is consistent with the available structural information. Consequently, even though the open-pore current is very different, the percentage block for a translocation event is similar for both pores. For example, the shortest peptide has a percentage block of 62% with α-hemolysin and 63% with aerolysin, whereas the values for the longest peptide are 78 and 76%, respectively.

Interaction of the Peptides with the Pores. The percentage block can be interpreted as an average measure of the fraction of the volume of the pore from which ions are excluded as the peptides are translocated (*8*, *9*). Therefore, I_2 increases as the peptides get longer. However, interactions between the peptide and pore must also be important because changes in the charge or charge density can influence I_2. For example, Fmoc-$D_3A_{14}K_2$ and Fmoc-$DA_{14}K$ for both types of pores show an increase in I_2 compared to Fmoc-$D_2A_{14}K_2$. Such an increase is particularly unexpected for Fmoc-$DA_{14}K$, which is shorter than Fmoc-$D_2A_{14}K_2$. The translocation times are also effected by changes in charge and charge density. With α-hemolysin, Fmoc-$D_3A_{14}K_2$ has a decreased T_2 compared to Fmoc-$D_2A_{14}K_2$, which is consistent with it being drawn through the pore down a voltage gradient. However, with aerolysin, T_2 increases, suggesting that the additional negative charge of Fmoc-$D_3A_{14}K_2$ causes a favorable interaction with the pore. For Fmoc-$DA_{14}K$ with both pores, T_2 is shorter than for Fmoc-$D_2A_{14}K_2$, consistent with a reduced interaction with the pore for the peptide with fewer charges.

Dipole Moment. An important finding of this work has been that the dipole moment can have a major effect on the transport characteristics of the polymer. From this perspective, it is much easier to alter the charge distribution on peptides than on DNA, which has previously been the subject of most research. Our initial experiments performed on peptides with the sequence $D_nA_xK_y$, without the Fmoc attached, yielded poor-quality data with a very small number

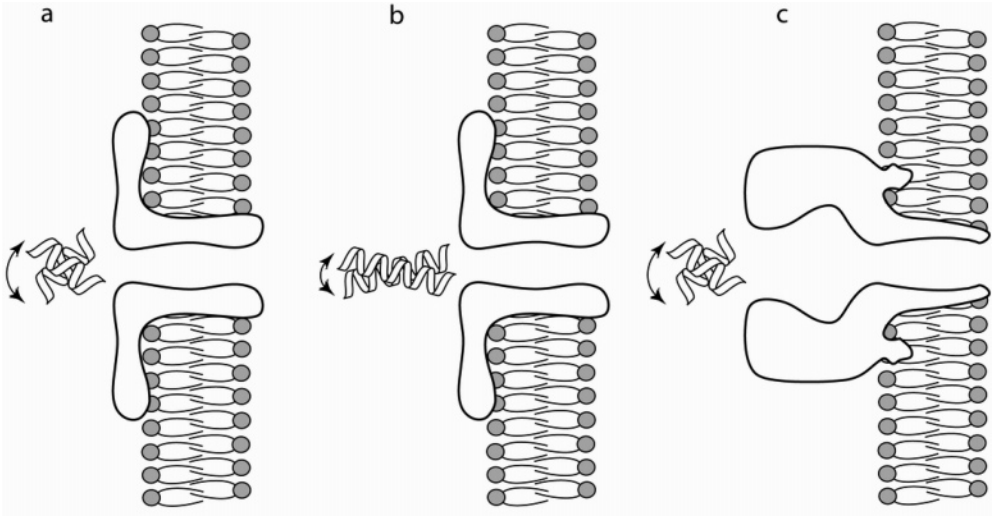

FIGURE 6: Effect of the dipole moment and length on the orientation and translocation of peptide molecules through α-hemolysin and aerolysin pores. (a) Short peptide has a small dipole moment and is therefore unlikely to be oriented correctly for the translocation through the aerolysin pore. (b) Long peptide has a larger dipole moment, which will help the molecule orient itself for translocation. (c) Presence of the vestibule of the α-hemolysin pore allows for a much larger capture radius than aerolysin, thus minimizing the number of bumping events for short peptide molecules.

of events (between 500 and 1000 events per experiment) (see the Supporting Information). Obviously, this was due to the lack of a net charge on the molecules making their interaction with the pore more diffusion-controlled than voltage-driven. Instead, the Fmoc-protected peptides brought very good results, with over 10 000 translocation events per experiment on each nanopore tested. For aerolysin, the ratio of bumping events/translocation events decreases as the dipole moment increases. For α-hemolysin, bumping events are only seen for Fmoc-$DA_{14}K$, which has the smallest dipole moment. Without an electric field, the peptide will rotate rapidly. In the presence of an electric field, the rotation will be restricted and the peptide is more likely to be oriented in the direction of the pore (see Figure 6). As the dipole moment increases, it becomes less probable for a peptide to bump into the entrance to the pore rather than translocate straight through. For α-hemolysin, we suggest that the presence of the vestibule allows for a much larger capture radius compared to aerolysin. In our previous analysis of collagen-like peptide translocation (*16*), events with a small i_{block} were eliminated from the analysis, but as shown here, these events can provide information about the orientation of the polymers. Our results also suggest that, for single-molecule experiments with solid-state pores, a conical aperture in front of the pore may be advantageous because it will reduce the number of bumping events and simplify the analysis.

Translocation Velocity. The longest peptide Fmoc-$D_2A_{22}K_2$ has a length of 44.5 Å as an α helix but would be more than 70 Å as an extended structure. Because this peptide has not reached the limiting velocity (Figure 5), its length inside the α-hemolysin pore is less than 50 Å. In other words, it seems unlikely that the α helices are unfolding before or during translocation. The limiting velocity of the translocating peptides is less than 10 nm/ms, which is 1−2 orders of magnitude slower than ssDNA under similar conditions. When the solution was cooled or glycerol was added (*14*), a further reduction in velocity by 1 or 2 orders of magnitude could be achieved. Such slow speeds may allow for the collection of more detailed structural information, but it seems unlikely that it will be sufficient for peptide sequencing without further improvements in the design of the pores.

ACKNOWLEDGMENT

H.-B. K. is the Canada Research Chair in Biomaterials, and J. S. L. holds a Senior Investigator award from the regional partnership program of CIHR.

SUPPORTING INFORMATION AVAILABLE

Figure S1, CD spectra of Fmoc-$D_2A_{10}K_2$ and Fmoc-$D_2A_{22}K_2$; Figure S2, t_{block} exponentials for $D_2A_{10}K_2$ with aerolysin; Figure S3, transport of $D_2A_{10}K_2$ through α-hemolysin and aerolysin pores. This material is available free of charge via the Internet at http://pubs.acs.org.

REFERENCES

1. Bezrukov, S. M., and Kasianowicz, J. J. (1993) Current noise reveals protonation kinetics and number of ionizable sites in an open protein ion channel, *Phys. Rev. Lett. 70*, 2352−2355.
2. Bezrukov, S. M., Vodyanoy, I., Brutyan, R. A., and Kasianowicz, J. J. (1996) Dynamics and free energy of polymers partitioning into a nanoscale pore, *Macromolecules 29*, 8517−8522.
3. Bezrukov, S. M., Vodyanoy, I., and Parsegian, V. A. (1994) Counting polymers moving through a single ion channel, *Nature 370*, 279−281.
4. Braha, O., Walker, B., Cheley, S., Kasianowicz, J. J., Song, L., Gouaux, J. E., and Bayley, H. (1997) Designed protein pores as components for biosensors, *Chem. Biol. 4*, 497−505.
5. Bustamante, J. O., Oberleithner, H., Hanover, J. A., and Liepins, A. (1995) Patch clamp detection of transcription factor translocation along the nuclear pore complex channel, *J. Membr. Biol. 146*, 253−261.
6. Vercoutere, W., and Akeson, M. (2002) Biosensors for DNA sequence detection, *Curr. Opin. Chem. Biol. 6*, 816−822.
7. Kasianowicz, J. J., Brandin, E., Branton, D., and Deamer, D. W. (1996) Characterization of individual polynucleotide molecules using a membrane channel, *Proc. Natl. Acad. Sci. U.S.A. 93*, 13770−13773.
8. Akeson, M., Branton, D., Kasianowicz, J. J., Brandin, E., and Deamer, D. W. (1999) Microsecond time-scale discrimination among polycytidylic acid, polyadenylic acid, and polyuridylic acid as homopolymers or as segments within single RNA molecules, *Biophys. J. 77*, 3227−3233.

9. Deamer, D. W., and Akeson, M. (2000) Nanopores and nucleic acids: Prospects for ultrarapid sequencing, *Trends Biotechnol. 18*, 147−151.
10. Meller, A., Nivon, L., Brandin, E., Golovchenko, J., and Branton, D. (2000) Rapid nanopore discrimination between single polynucleotide molecules, *Proc. Natl. Acad. Sci. U.S.A. 97*, 1079−1084.
11. Li, J., Stein, D., McMullan, C., Branton, D., Aziz, M. J., and Golovchenko, J. A. (2001) Ion-beam sculpting at nanometre length scales, *Nature 412*, 166−169.
12. Li, J., Gershow, M., Stein, D., Brandin, E., and Golovchenko, J. A. (2003) DNA molecules and configurations in a solid-state nanopore microscope, *Nat. Mater. 2*, 611−615.
13. Storm, A. J., Chen, J. H., Ling, X. S., Zandbergen, H. W., and Dekker, C. (2003) Fabrication of solid-state nanopores with single-nanometre precision, *Nat. Mater. 2*, 537−540.
14. Fologea, D., Uplinger, J., Thomas, B., McNabb, D. S., and Li, J. (2005) Slowing DNA translocation in a solid-state nanopore, *Nano Lett. 5*, 1734−1737.
15. Movileanu, L., Schmittschmitt, J. P., Scholtz, J. M., and Bayley, H. (2005) Interactions of peptides with a protein pore, *Biophys. J. 89*, 1030−1045.
16. Sutherland, T. C., Long, Y. T., Stefureac, R. I., Bediako-Amoa, I., Kraatz, H. B., and Lee, J. S. (2004) Structure of peptides investigated by nanopore analysis, *Nano Lett. 4*, 1273−1277.
17. Perutz, M. F., Pope, B. J., Owen, D., Wanker, E. E., and Scherzinger, E. (2002) Aggregation of proteins with expanded glutamine and alanine repeats of the glutamine-rich and asparagine-rich domains of Sup35 and of the amyloid *β*-peptide of amyloid plaques, *Proc. Natl. Acad. Sci. U.S.A. 99*, 5596−5600.
18. Howard, S. P., and Buckley, J. T. (1986) Molecular cloning and expression in *Escherichia coli* of the structural gene for the hemolytic toxin aerolysin from *Aeromonas hydrophila*, *Mol. Gen. Genet. 204*, 289−295.
19. Howard, S. P., Garland, W. J., Green, M. J., and Buckley, J. T. (1987) Nucleotide sequence of the gene for the hole-forming toxin aerolysin of *Aeromonas hydrophila*, *J. Bacteriol. 169*, 2869−2871.
20. Moniatte, M., vanderGoot, F. G., Buckley, J. T., Pattus, F., and vanDorsselaer, A. (1996) Characterisation of the heptameric pore-forming complex of the *Aeromonas* toxin aerolysin using MALDI−TOF mass spectrometry, *Febs Lett. 384*, 269−272.
21. Wilmsen, H. U., Pattus, F., and Buckley, J. T. (1990) Aerolysin, a hemolysin from *Aeromonas hydrophila*, forms voltage-gated channels in planar lipid bilayers, *J. Membr. Biol. 115*, 71−81.
22. Song, L. Z., Hobaugh, M. R., Shustak, C., Cheley, S., Bayley, H., and Gouaux, J. E. (1996) Structure of staphylococcal α-hemolysin, a heptameric transmembrane pore, *Science 274*, 1859−1866.
23. Parker, M. W., Buckley, J. T., Postma, J. P. M., Tucker, A. D., Leonard, K., Pattus, F., and Tsernoglou, D. (1994) Structure of the *Aeromonas* toxin proaerolysin in its water-soluble and membrane-channel states, *Nature 367*, 292−295.
24. Meller, A., Nivon, L., and Branton, D. (2001) Voltage-driven DNA translocations through a nanopore, *Phys. Rev. Lett. 86*, 3435−3438.
25. Chan, W. (2000) *Fmoc Solid-Phase Peptide Synthesis: A Practical Approach*, Oxford University Press, New York.
26. Meller, A., and Branton, D. (2002) Single molecule measurements of DNA transport through a nanopore, *Electrophoresis 23*, 2583−2591.
27. Heins, E. A., Siwy, Z. S., Baker, L. A., and Martin, C. R. (2005) Detecting single porphyrin molecules in a conically shaped synthetic nanopore, *Nano Lett. 5*, 1824−1829.
28. Creighton, T. E. (1993) *Proteins. Structure and Molecular Properties*, 2nd ed., pp 143−145, W. H. Freeman and Company, New York.

BI0604835